

Article

Kinetics of the Gas-Phase Reaction of Hydroxyl Radicals with Dimethyl Methylphosphonate (DMMP) over an Extended Temperature Range (273–837 K)

Xiaokai Zhang ¹, Daria A. Barkova ², Pavel V. Koshlyakov ² , Ilya E. Gerasimov ², Evgeni N. Chesnokov ² and Lev N. Krasnoperov ^{1,*}

¹ Department of Chemistry and Environmental Science, New Jersey Institute of Technology, Newark, NJ 07102, USA; zhangxz458@njit.edu

² Institute of Chemical Kinetics and Combustion, Siberian Branch of Russian Academy of Sciences, 630090 Novosibirsk, Russia; d.plastinina@g.nsu.ru (D.A.B.); pvk@kinetics.nsc.ru (P.V.K.); gerasimov@kinetics.nsc.ru (I.E.G.); chesnok@kinetics.nsc.ru (E.N.C.)

* Correspondence: lev.n.krasnoperov@njit.edu or chesnokov@kinetics.nsc.ru

Abstract: The kinetics of the reaction of hydroxyl radical (OH) with dimethyl methylphosphonate (DMMP, (CH₃O)₂CH₃PO) (reaction 1) OH + DMMP → products (1) was studied at the bath gas (He) pressure of 1 bar over the 295–837 K temperature range. Hydroxyl radicals were produced in the fast reaction of electronically excited oxygen atoms O(¹D) with H₂O. The time-resolved kinetic profiles of hydroxyl radicals were recorded via UV absorption at around 308 nm using a DC discharge H₂O/Ar lamp. The reaction rate constant exhibits a pronounced V-shaped temperature dependence, negative in the low temperature range, 295–530 K (the rate constant decreases with temperature), and positive in the elevated temperature range, 530–837 K (the rate constant increases with temperature), with a turning point at 530 ± 10 K. The rate constant could not be adequately fitted with a standard 3-parameter modified Arrhenius expression. The data were fitted with a 5-parameter expression as: $k_1 = 2.19 \times 10^{-14} (T/298)^{2.43} \exp(15.02 \text{ kJ mol}^{-1} / RT) + 1.71 \times 10^{-10} \exp(-26.51 \text{ kJ mol}^{-1} / RT) \text{ cm}^3 \text{ molecule}^{-1} \text{ s}^{-1}$ (295–837 K). In addition, a theoretically predicted pressure dependence for such reactions was experimentally observed for the first time.

Keywords: kinetics; hydroxyl; radical; dimethyl methylphosphonate; DMMP; laser photolysis; transient absorption; V-shaped temperature dependence; pressure dependence



Citation: Zhang, X.; Barkova, D.A.; Koshlyakov, P.V.; Gerasimov, I.E.; Chesnokov, E.N.; Krasnoperov, L.N. Kinetics of the Gas-Phase Reaction of Hydroxyl Radicals with Dimethyl Methylphosphonate (DMMP) over an Extended Temperature Range (273–837 K). *Molecules* **2022**, *27*, 2301. <https://doi.org/10.3390/molecules27072301>

Academic Editor: Jose C. Corchado

Received: 18 February 2022

Accepted: 28 March 2022

Published: 1 April 2022

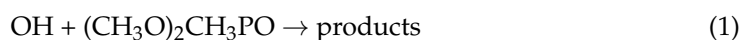
Publisher's Note: MDPI stays neutral with regard to jurisdictional claims in published maps and institutional affiliations.



Copyright: © 2022 by the authors. Licensee MDPI, Basel, Switzerland. This article is an open access article distributed under the terms and conditions of the Creative Commons Attribution (CC BY) license (<https://creativecommons.org/licenses/by/4.0/>).

1. Introduction

During the last decades, organophosphorus compounds have been recognized as efficient flame retardants even at relative low concentrations [1–10]. On the other hand, organophosphorus compounds also exist in the environment as pesticides, insecticides, etc. [11,12]. Detailed mechanisms of the flame retardancy as well of the destruction of these compounds in the environment require detailed information on the kinetics of the elementary reactions of these compounds in the reaction mechanisms. Currently, such data, even for the reactions with the major oxidation species, hydroxyl radical (OH), are very sparse. Specifically, for the target reaction of this study, reaction of hydroxyl radical with dimethyl methylphosphonate, DMMP, (CH₃O)₂CH₃PO (Equation (1)), only a single indirect kinetic study exists [13].



In this single gas phase indirect kinetic study the rate of reaction (1) was measured relative to the rate of reaction of hydroxyl radicals with n-butyl ether (n-C₄H₉)₂O over the temperature range 283–348 K. A negative temperature dependence was observed in this temperature range (reaction slows down with temperature). Similar behavior

was previously observed for the reaction of hydroxyl radical with trimethyl phosphate (TMP, $(\text{CH}_3\text{O})_3\text{PO}$) [14], where the negative temperature dependence at low temperatures switched to a positive temperature dependence at elevated temperatures, resulting in a V-shaped temperature dependence. Such a behavior was predicted in the interpretation of the kinetics of the reaction $\text{CH}_3 + \text{HBr}$ [15,16] based on the concept of “negative” or “submerged” reaction barrier.

The reaction was also studied in solution using pulsed radiolysis; using relative rate technique, important mechanistic conclusions have been derived [17].

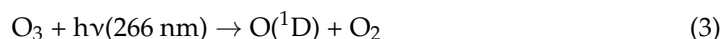
In this work, the kinetics of reaction (1) was investigated using pulsed laser photolysis combined with transient UV absorption over an extended temperature range (295–837 K). A peculiar V-shaped temperature dependence was observed similar to that previously reported for the reaction of OH with trimethyl phosphate (TMP) [14]. Pressure dependence was also observed in the pressure range 0–30 bar, as predicted in the theoretical study [16].

The measurements were performed in two laboratories, Institute of Chemical Kinetics and Combustion, ICKC, Novosibirsk, Russia and New Jersey Institute of Technology, NJIT, Newark, USA. In both studies hydroxyl radicals (OH) were formed using fast reaction of electronically excited atoms $\text{O}(^1\text{D})$ with H_2O molecules [18,19].

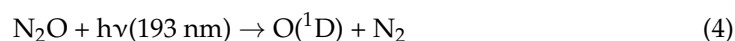


Reaction 2 is very fast, the reaction of $\text{O}(^1\text{D})$ with H_2O requires only a few collisions (the rate constant $k_{2a} = 2.0 \times 10^{-10} \text{ cm}^3 \text{ molecule}^{-1} \text{ s}^{-1}$ at 298 K) [19]. Moreover, due to the relatively strong O-H bond in the water molecule, reaction (2) produces fewer vibrational and rotational excitations, compared to other reactions with H-containing molecules. Moreover, reaction (2) produces two hydroxyl radicals per one excited oxygen atom, and no other free radical species, which can complicate the reaction mechanism. Therefore reaction (2) was chosen as the source of hydroxyl radicals in this study.

At the Institute of Chemical Kinetics and Combustion (ICKC), electronically excited oxygen atoms were produced by photolysis of ozone at 266 nm:



The temperature range of this study was 273–470 K, the highest temperature was limited by the thermal stability of ozone. The temperature range was significantly expanded using a different photolysis system, available at NJIT. Specifically, to produce excited oxygen atoms, photolysis of N_2O at 193 nm (ArF excimer laser) was used. N_2O has much better thermal stability, compared with that of ozone. The replacement of excited oxygen atom photochemical precursor, allowed raising the upper temperature of the available temperature range to 837 K.



2. Experimental

The experimental set-ups at the ICKC and NJIT used in the study are similar. Both are based on pulsed laser photolysis coupled with a time resolved transient absorption spectroscopy. The only major difference is in the different photolysis systems used to produce excited oxygen atoms, $\text{O}(^1\text{D})$.

2.1. Experimental: ICKC

The experimental set-up at ICKC was described previously [14,20]. Ozone produced on-line using a corona discharge dielectric barrier ozonator is mixed with other reactants in a flow system. Gas mixture of 10% O_2 in He was passed through the ozonator. The typical degree of conversion of O_2 to O_3 was about 7%. The ozone concentration in the reactor was determined accurately and directly in situ by absorbance at the 253 nm using a mercury resonance lamp using accurately known absorption coefficients. Ozone is photolyzed at 266 nm (4th harmonic

of an Nd:YAG laser, Lotis Tii, model: LS-2137U). Temporal profiles of OH absorption of light produced by a DC discharge hydroxyl lamp (multiline around 308 nm) passed through a monochromator are digitized, accumulated and stored using a digital oscilloscope. The typical concentration of ozone was ca. 3.44×10^{14} molecule cm^{-3} . Typical concentration of molecular oxygen, O_2 , was ca. 8.2×10^{15} molecule cm^{-3} . Hydroxyl radicals were generated in the reaction of excited oxygen atoms $\text{O}(^1\text{D})$ with water molecules (reaction (2)). Typical concentration of water molecules was ca. 2.5×10^{16} molecule cm^{-3} .

Hydroxyl radicals were monitored via absorption of light generated by a low pressure DC discharge lamp in a $\text{H}_2\text{O}/\text{Ar}$ mixture. The OH lamp is a quartz tube, with two metal fittings at the ends. Argon, saturated with water vapor at ca. 1 bar pressure and ambient temperature, was pumped through the lamp at 40 Torr (5.33 kPa). DC voltage of 5 kV was applied to the metal fittings of the OH lamp via a ballast resistor, the electric current was 30 mA. The light emitted from the lamp passed through the reactor was focused on the entrance slit of a monochromator (Carl Zeiss, SPM2). The spectral width was set ca. 12 nm to select a bunch of ca. 20 emission lines of hydroxyl radical around 308 nm. The temperature and pressure dependences of the apparent absorption cross-section of hydroxyl radical obtained with such a lamp as well as the curves-of-growth were studied in detail in the experiments as well as via modeling in previous studies [21–23]. For the optical arrangement at ICKC, used in the current study, the low pressure low absorbance (<2%) experimentally determined apparent absorption cross section of OH was 7.2×10^{-17} $\text{cm}^2\text{molecule}^{-1}$ at 293 K.

A heated metal flow reactor, 10 cm long with an inner diameter of 8 mm with fused quartz windows, was used. Before entering the heated reactor, the flowing reaction mixture was preheated to the reactor temperature via placing the 2 m entering tube as well as the reactor in a common heater. The temperature of the reactor ranged from 273 to 473 K. The pressure in the cell was ca. 12–15 Torr (1600–2000 Pa) above ambient atmospheric pressure and was in the range 750–775 Torr (99.98–103.30 kPa).

The main bath gas (helium) flowrate was measured with an SMC PFMV510-1 flowmeter. The main flow rate was 1000 sccm. The flowrate of the O_2/He mixture was measured before entering the ozonator by an MF Matheson 8141 flow meter; the flow rate was ca. 4 sccm. Measurements and control of small helium flows passing through a two-stage water saturator was done using a TylanFC 260 mass flow controller. This helium flow was about 44 sccm.

The reactant (dimethyl methylphosphonate, DMMP) was introduced using an Agilent chromatographic syringe with a volume of 25 μL driven by a stepper motor. DMMP was supplied to the evaporator, which in turn was purged with the main helium flow. The flow rate of liquid DMMP ranged from 0 to 0.46 $\mu\text{L}/\text{min}$ which, after evaporation, corresponds to 0–0.11 sccm. The DMMP concentration in the reactor was varied from 0 to 2×10^{15} cm^{-3} .

2.2. Reagents (ICKC)

The purity of the gases used in the work were: He > 99.995%, O_2 grade pure > 99.95%, H_2O was deionized, the resistance was 17 MOhm cm, and Ar > 99.999%. DMMP was purchased from Aldrich (purity >97%).

2.3. Experimental: NJIT

The experimental set-up used at NJIT is described in detail in previous publications [21–26]. Hydroxyl radicals were generated in pulsed photolysis of N_2O in the presence of water vapor at 193.3 nm (ArF excimer laser). The importance of different channels of the photodissociation process (reaction (4)) as well as of the subsequent reaction of $\text{O}(^1\text{D})$ with H_2O (reaction (2)) are also discussed in detail in previous publications [20–23].

The kinetics of hydroxyl radical decay was monitored by absorption in the UV (multiline at ca. 308 nm using low pressure $\text{H}_2\text{O}/\text{Ar}$ DC discharge lamp). Before entering the reactor, the laser beam was formed (to provide uniformity) with two lenses. The beam uniformity across the reactor cross-section was $\pm 7.3\%$ from the mean value. The gas flow

rates were controlled by mass flow controllers (Brooks, model 5850). The total flow rates of the reactant mixtures with helium were in the range 11–12 sccs. Additional flush flows to the reactor windows were 2 sccs. A precision syringe pump (Harvard Apparatus, model PHD 4400) was used to inject liquid water. Pure liquid DMMP was used via injection using another syringe pump. The injection was performed via corresponding capillary tubes through an evaporator (kept at 90 °C) and, subsequently, to the reactor. In this way, steady flows of H₂O and DMMP vapor were achieved. The total flow rate of these two liquids were kept constant at each given temperature, ranges from 6 to 11 μL/min, provided approximately the same concentration of H₂O. The equivalent gas flow rate of DMMP in standard cubic centimeters per minute (scm) was calculated based on the volumetric flowrate of the solution, based on the ideal gas law.

The concentrations of the precursors used were $(1.94\text{--}3.24) \times 10^{17}$ (H₂O), $(3.23\text{--}7.70) \times 10^{16}$ (N₂O) and $(0\text{--}10) \times 10^{14}$ (DMMP) molecule cm⁻³.

The absolute concentrations of OH radicals were determined based on the photon flux inside the reactor, the absorption cross-section of N₂O at 193.3 nm and the efficiency of conversion of O(¹D) atoms produced in the photolysis of N₂O to OH radicals. The absorption cross-section of N₂O is accurately known at 298 and 1 bar, at other conditions, the cross-sections of N₂O were measured in previous works [20–23]. The model used for the calculations of the efficiency of conversion of excited O(¹D) atom to OH radicals as well as the in situ laser light actinometry are described in detail in previous studies. The approach is based on the monitoring of ozone formation at 253.6 nm in the photolysis of N₂O/O₂/N₂ mixtures at 1 bar and 298 K. The photolysis laser photon fluence inside the reactor was varied in the range of $(4\text{--}9) \times 10^{15}$ photon cm⁻²pulse⁻¹. The initial concentrations of hydroxyl radicals were in the range $(1.4\text{--}2.7) \times 10^{13}$ molecule cm⁻³. All experiments were performed at 1 bar (He) pressure over 295–837 K temperature range.

2.4. Reagents (NJIT)

Helium used in the experiments was BIP Helium from Airgas with 99.9999% purity with reduced oxygen content (<10 ppb). UHP oxygen was obtained from Matheson TriGas (99.98% purity). Certified mixture of N₂O in He (2.50%, accuracy ±2%) obtained from Matheson Tri-Gas was used. Purified water (Milli-Q) with TOC less than 5 ppb) was degassed by freeze-pump-thaw cycles and used as a reactant supplied by a syringe pump (Harvard Apparatus PHD 4400) as well as in the low pressure H₂O/Ar discharge hydroxyl monitoring lamp. UHP argon obtained from Matheson TriGas (99.999% purity) was used in the H₂O/Ar lamp. DMMP was purchased from Aldrich (purity >98%).

3. Results

Sample OH absorption profiles obtained in the O₃/O₂/H₂O/DMMP/He + 266 nm and N₂O/H₂O/DMMP/He +193 nm are shown in Figures 1 and 2, respectively. The increase of the absorption in the figures corresponds to the formation of hydroxyl in reaction (2). The reaction of O(¹D) atoms with H₂O is extremely fast (the rate constant, $k = 1.8 \times 10^{-10}$ cm³/s) [18,19], therefore the conversion time of excited oxygen atoms did not exceed 1 μs.

Decay of the OH concentration is due to the different reactions of OH, including OH radical self-reaction, decay on the walls as well as the target reaction with DMMP. The secondary reactions of the products of reaction (1) might also contribute to the decay rates. In contrast to our previous studies of elementary reactions of hydroxyl radical and other radical species, where a system of differential equations that corresponds to the reaction mechanism was numerically solved and the resulting profiles were fitted to the experimental, a simplified analysis was accepted in this work. For reaction (1), currently no information about the products, branching ratios and the rate constants of subsequent reactions of the products of reaction (1), is available, and the previously used rigorous approach is not feasible. In lieu of the lack of a detailed reaction mechanism, no integrated

kinetic decay curves could be obtained. Therefore, the method of the initial rates also widely used in chemical kinetics was applied as described below.

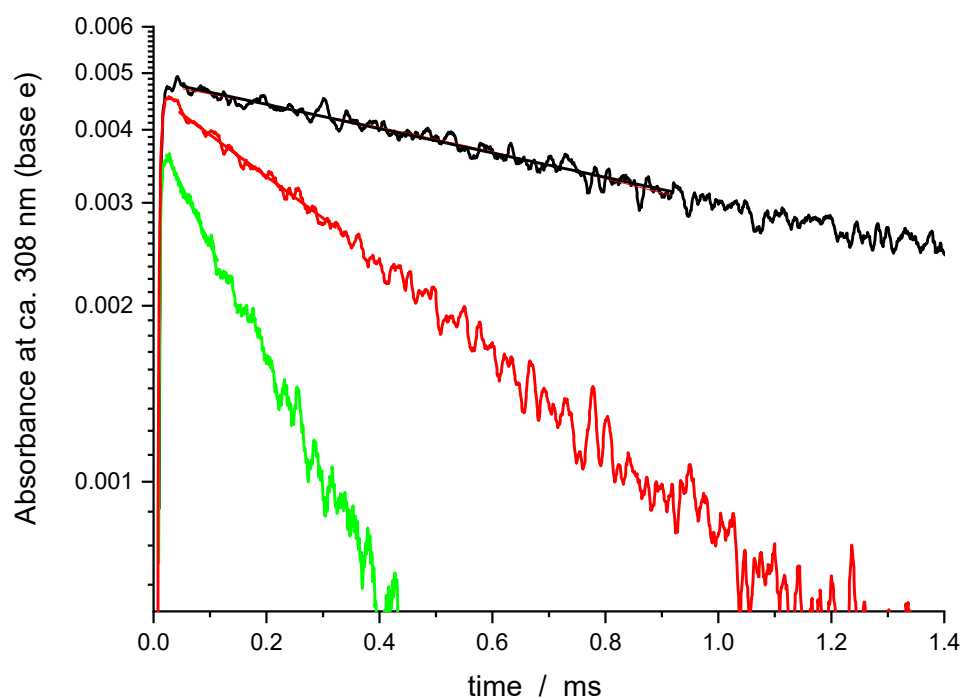


Figure 1. Sample transient absorption signals of OH in a $\text{O}_3/\text{O}_2/\text{H}_2\text{O}/\text{He}$ mixture at 266 nm and $T = 411 \text{ K}$. $[\text{O}_3] = 3.43 \times 10^{14}$, $[\text{H}_2\text{O}] = 2.3 \times 10^{16}$, $[\text{He}] = 1.8 \times 10^{19}$. Black—without DMMP, red— $[\text{DMMP}] = 3.67 \times 10^{14} \text{ molecule cm}^{-3}$, green— $[\text{DMMP}] = 10.9 \times 10^{14} \text{ molecule cm}^{-3}$. Solid lines—exponential fits of ca. 1/3 of the initial amplitude (see text).

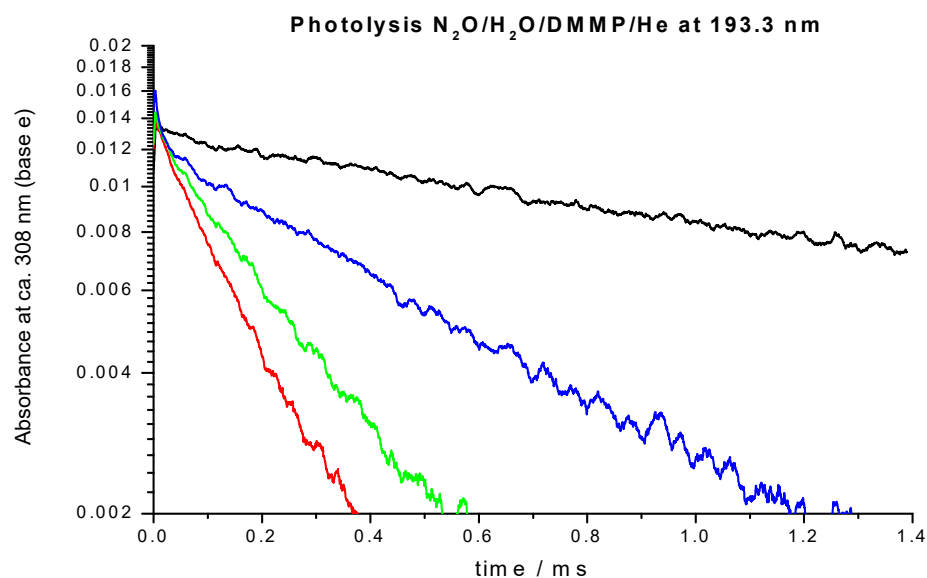


Figure 2. Sample UV absorption profiles of OH radical (multiline at ca. 308 nm). Photolysis of $\text{N}_2\text{O}/\text{H}_2\text{O}/\text{DMMP}/\text{He}$ mixtures at 193.3 nm. $T = 365 \text{ K}$, $p = 1 \text{ bar}$. $[\text{N}_2\text{O}] = 4.49 \times 10^{16} \text{ molecule cm}^{-3}$, $[\text{H}_2\text{O}] = 2.91 \times 10^{17} \text{ molecule cm}^{-3}$, $[\text{N}_2\text{O}]/[\text{H}_2\text{O}] = 0.154$. Black— $[\text{DMMP}] = 0$, blue— $[\text{DMMP}] = 1.92 \times 10^{14} \text{ molecule cm}^{-3}$, green— $[\text{DMMP}] = 5.76 \times 10^{14} \text{ molecule cm}^{-3}$, and red— $[\text{DMMP}] = 9.59 \times 10^{14} \text{ molecule cm}^{-3}$.

After formation of hydroxyl radicals in the reaction of excited oxygen atoms with water molecules, the radicals are consumed in the target reaction (1) as well as in the side

reactions discussed above. Therefore, at short times the rate constant of consumption, k' , is written as:

$$k' = \left(-\frac{1}{[\text{OH}]_0} \frac{d[\text{OH}]}{dt} \right)_{t=0} \quad (5)$$

$$k' = k_1' + k_0 \quad (6)$$

$$k_1' = k_1[\text{DMMP}] \quad (7)$$

where k' is the “initial slope rate constant” defined by Equation (5), $k_1' = k_1[\text{DMMP}]$ is the pseudo-first order rate constant of the target reaction, and k_0 accounts for all other processes. In the evaluation of the initial slopes, the initial fractions of the decay curves should be properly fitted. There are numerous functions, including just the linear one, which can be used for this purpose. In the case of pseudo-first order decays, the decay profiles are exponential. Therefore, the exponential decay function was chosen to evaluate the initial decay rates, since it provides unbiased estimation of the “initial slopes” for pseudo-first order processes.

To evaluate the “initial slope” rate constant, the initial portion of the decay profiles (about 1/3 of the amplitude) was fitted with exponential function

$$[\text{OH}] = [\text{OH}]_0 \exp(-k't) \quad (8)$$

Then plotting the “initial slope rate constant” k' vs. the reactant concentration $[\text{DMMP}]$ one expects to obtain a straight line whose slope yields the rate constant of the target reaction (1), and the intercept the contribution of other processes (such as self-reaction) at the initial stage of the reaction.

The rate constant of the self-reaction of hydroxyl radicals is well characterized [20–22], and its contribution into the initial decay is easily assessable. Assessment of the potential interference of the reactions with the products of the target reaction (1) is not straightforward. The only possibility is to use very low initial concentrations of OH, to reduce the possible role of such processes. The maximum values of k' were about $10,000 \text{ s}^{-1}$. The majority of the experiments were performed with the initial absorbance of OH radicals not exceeding 1.5%, which translates to the initial concentrations of the radicals of ca. $2 \times 10^{13} \text{ molecule cm}^{-3}$. Assuming that the rate constants of the secondary reactions of OH with the presumable free radical products of reaction (1) do not exceed a typical value for barrierless radical-radical reactions of $3 \times 10^{-11} \text{ cm}^3 \text{ molecule}^{-1} \text{ s}^{-1}$, such initial concentrations might contribute up to $ca. 3 \times 10^{-11} \times 2 \times 10^{13} = 600 \text{ s}^{-1}$, i.e., ca 6% of the maximum decay rate. Only ca. 1/3 of the initial amplitude was used in the decay fits to evaluate the “initial slope” rate constant, so that the above estimate of the contribution of the reactions with the reaction products is reduced further by a factor of 3, the contribution does not exceed 2% of the maximum rate.

Sample dependences of the “initial slope rate constant” k' , on the reactant (DMMP) concentration are shown in Figure 3. The dependences are linear, the slopes yield the rate constants of the target reaction (1). The negative temperature dependence (the decrease of the reaction rate with temperature, negative apparent activation energy) is apparent in the low temperature range. In the high temperature range, the rate constant increases with temperature (positive temperature dependence, positive apparent activation energy).

The results of all measurements where ozone was used as photolytic source of excited oxygen atoms are listed in Table 1. The negative temperature dependence in the low temperature range is apparent. As it was already mentioned, the temperature range of the study was significantly extended by using N_2O as a photolytic source of excited oxygen atoms, $\text{O}(^1\text{D})$. N_2O has much better thermal stability, thus the upper temperature of the experiments was raised to 837 K. Sample decay profiles obtained in the photolysis system $\text{N}_2\text{O}/\text{H}_2\text{O}/\text{TMP}/\text{He} + h\nu(193 \text{ nm})$ at 365 K at several concentrations of the reactant, DMMP, are shown in Figure 2. Sample data processing via plotting the “initial slope” rate constant k' vs. concentration of the reactant, TMP, is shown in Figure 3. The negative

temperature dependence at low temperatures turns to a positive dependence at higher temperatures. All the results together with the experimental conditions are summarized in Tables 1 and 2 and are shown in Figure 4 together with the results of the only previous (indirect) study [13].

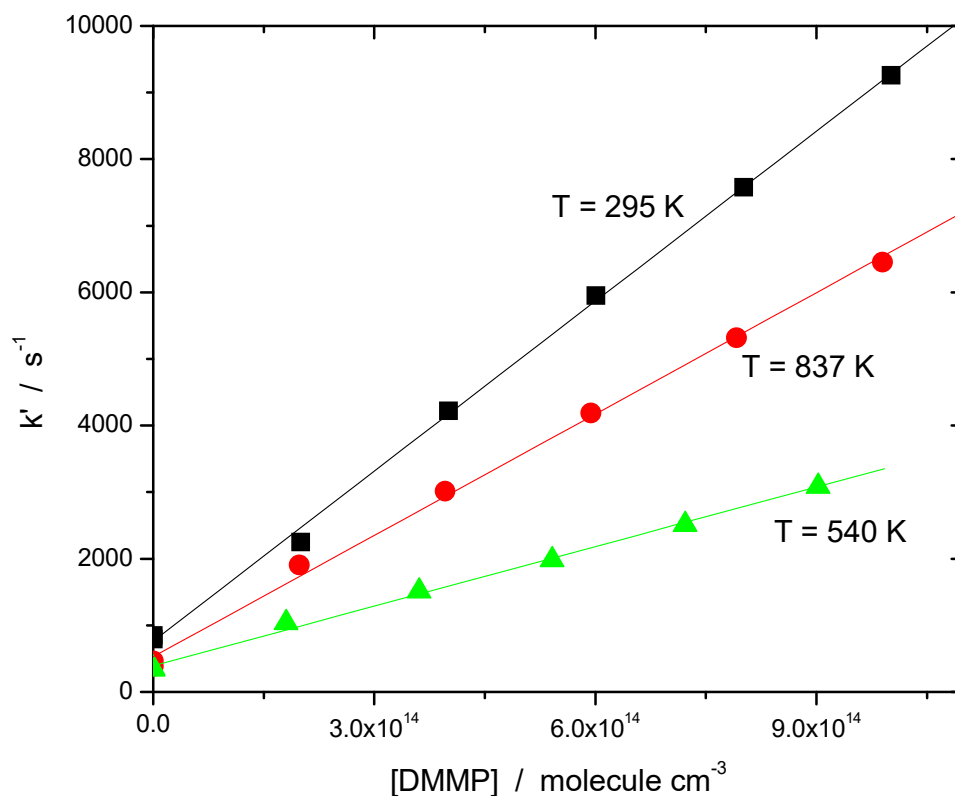


Figure 3. Sample dependences of the “initial slope rate constant, k' ” on concentration of DMMP at three temperatures (low, high and an intermediate). Photolysis of $N_2O/H_2O/DMMP/He$ mixtures at 193 nm. The slopes yield the rate constants of the target reaction (1). Negative temperature dependence (decrease of the rate constant with temperature) at low temperatures as well as positive temperature dependence (increase of the rate constant with temperature) at high temperatures are apparent.

The rate constant could not be adequately fitted with a standard 3-parameter modified Arrhenius expression. To provide an accurate fit to the experimental data, a minimum of five parameters are required. The data were fitted with a 5-parameter expression as:

$$k_1 = 2.19 \times 10^{-14} (T/298)^{2.43} \exp(15.02 \text{ kJ mol}^{-1}/RT) + 1.71 \times 10^{-10} \exp(-26.51 \text{ kJ mol}^{-1}/RT) \quad (295\text{--}837 \text{ K}) \quad (9)$$

The modified transition state theory (MTST) that describes application of the concept of the transition state to the reactions where the ground state of the transition state lies below the ground state of the reactants (“negative barrier”, “submerged barrier”) explains not only the negative temperature dependence of the reaction rate at low temperatures, but also predicts the turning point in the temperature dependence (“V-shape”) and possible pressure dependence [16,26]. The theory predicts lower rate constant at low pressures, k_{MTST} , compared to a larger rate constant at high pressures, k_{TST} . The transition is expected at high pressures (tens and hundreds of bar), the impact of pressure is expected to be larger at low temperatures.

The V-shaped temperature dependence was observed in this study (OH + dimethyl methylphosphonate) as well as in the previous study, OH + trimethyl phosphate [14]. Similar dependences are expected for other organophosphorus compounds containing methoxy groups.

Table 1. Experimental conditions for the experiments with O₃/O₂/H₂O/DMMP/He + 266 nm. All measurements at 1.00 ± 0.02 bar.

Temperature/K	[O ₃]/10 ¹⁴ Molecule cm ⁻³	[O ₂]/10 ¹⁵ Molecule cm ⁻³	[H ₂ O]/10 ¹⁶ Molecule cm ⁻³	[He]/10 ¹⁹ Molecule cm ⁻³	[DMMP]/10 ¹⁴ Molecule cm ⁻³	k'/10 ³ s ⁻¹	k/10 ⁻¹² cm ³ Molecule ⁻¹ s ⁻¹
299	4.57	9.80	3.38	2.44	0	0.467	
299	4.57	9.80	3.38	2.44	4.70	5.03	
299	4.57	9.80	3.38	2.44	9.41	9.98	
299	4.57	9.77	3.37	2.44	14.1	15.2	10.5
299	4.57	9.75	3.37	2.44	18.73	19.9	
299	4.57	9.68	3.34	2.44	23.2	25.4	
299	4.54	9.69	3.42	2.44	0	0.511	
299	4.54	9.62	3.4	2.44	4.73	5.55	
299	4.54	9.46	3.38	2.44	9.42	9.83	
299	4.54	9.32	3.33	2.44	13.9	14.3	9.85
299	4.54	10.31	3.51	2.44	19.6	19.1	
299	4.54	10.35	3.49	2.44	24.3	23.9	
328	2.78	9.05	3.30	2.26	0	0.450	
328	2.78	8.79	3.14	2.26	4.37	3.22	
328	2.78	8.66	3.10	2.26	8.61	6.25	
328	2.78	8.51	3.08	2.26	12.8	8.33	6.70
328	2.78	8.47	3.07	2.26	17.0	13.2	
328	2.78	8.29	3.04	2.26	21.1	14.2	
365	1.78	8.19	2.77	2.02	0	0.452	
365	1.78	8.18	2.74	2.02	3.97	1.95	
365	1.78	8.22	2.67	2.02	7.98	4.16	4.75
365	1.78	8.08	2.65	2.02	11.9	5.88	
365	1.78	8.03	2.63	2.02	15.7	7.69	
365	1.78	7.83	2.60	2.02	19.4	8.33	
365	3.97	8.15	2.57	2.00	0	0.452	
365	3.97	7.99	2.63	2.00	4.02	2.32	
365	3.97	7.95	2.62	2.00	8.00	4.16	
365	3.97	7.84	2.61	2.00	11.9	6.66	5.06
365	3.97	7.70	2.60	2.00	15.8	8.33	
365	3.97	7.53	2.62	2.00	19.6	9.09	
365	3.97	8.72	2.67	2.00	0	0.413	
365	3.97	8.63	2.64	2.00	12.4	6.66	
365	3.97	8.46	2.62	2.00	16.4	9.09	
365	3.97	8.30	2.60	2.00	20.4	11.1	5.04
365	3.97	8.16	2.58	2.00	24.3	12.5	
365	3.97	7.93	2.54	2.00	11.9	6.66	
365	3.97	7.79	2.53	2.00	23.8	12.7	
411	3.44	7.50	2.31	1.80	0	0.450	
411	3.44	7.64	2.30	1.80	3.67	1.75	
411	3.44	7.34	2.29	1.80	7.30	3.03	
411	3.44	7.20	2.27	1.80	10.8	4.54	3.99
411	3.44	7.06	2.25	1.80	14.3	6.25	
411	3.44	7.02	2.24	1.80	17.8	7.14	
470	1.88	6.44	1.99	1.59	0	0.478	
470	1.88	6.39	1.99	1.59	3.22	1.38	
470	1.88	6.28	1.99	1.59	6.40	2.22	
470	1.88	6.56	1.98	1.59	9.55	3.33	3.16
470	1.88	5.39	1.96	1.58	12.6	4.16	
470	1.88	6.23	1.95	1.59	15.6	5.55	

However, such pressure effect on a rate of a “simple metathesis reaction” was not yet observed. We performed pressure dependent measurements over the pressure range 1–30 bar at the lowest temperature, currently available (ambient). The results are shown in Figure 5. The rate constant increases with pressure from 0.87×10^{-11} at 1 bar to 1.77×10^{-11} cm³molecule⁻¹s⁻¹ at 30 bar.

The data were fitted using the following expression:

$$k = k_0 + (k_{\text{inf}} - k_0)(p/p_0)/(1 + p/p_0) \quad (10)$$

The expression (10) corresponds to a simple model, where all relaxation processes are described by a single parameter, p_0 , the transition pressure. The results of the fit are: the low-pressure limit rate constant, $k_0 = k_{\text{MTST}} = (7.64 \pm 0.12)10^{-12}$ cm³molecule⁻¹s⁻¹, the high-pressure limit rate constant, $k_{\text{inf}} = k_{\text{TST}} = (2.25 \pm 0.05)10^{-11}$ cm³molecule⁻¹s⁻¹, and the transition pressure $p_0 = (15.2 \pm 1.2)$ bar. The study is planned to be extended to a wider pressure range (0–100 bar) as well to lower temperatures (down to ca. -80 °C).

Table 2. Experimental conditions for the experiments with N₂O/H₂O/DMMP + 193.3 nm. All measurements at 1.00 ± 0.02 bar (He).

Temperature/K	[H ₂ O]/10 ¹⁷ Molecule cm ⁻³	[N ₂ O]/10 ¹⁶ Molecule cm ⁻³	[DMMP]/10 ¹⁴ Molecule cm ⁻³	k'/10 ³ s ⁻¹	k/10 ⁻¹² cm ³ Molecule ⁻¹ s ⁻¹
295	3.03	3.23	0	0.847	
295	3.03	3.23	10.0	9.25	
295	3.03	3.23	8.0	7.57	
295	3.03	3.23	6.0	5.95	8.51
295	3.03	3.23	4.0	4.21	
295	3.03	3.23	2.0	2.24	
295	3.03	3.23	0	0.794	
323	2.98	7.70	0	0.448	
323	2.98	7.70	7.56	5.61	
323	2.98	7.70	6.05	4.60	
323	2.98	7.70	4.54	3.43	6.82
323	2.98	7.70	3.02	2.34	
323	2.98	7.70	1.51	1.51	
323	2.98	7.70	0	0.442	
365	2.91	4.49	0	0.463	
365	2.91	4.49	9.59	5.68	
365	2.91	4.49	7.68	4.58	5.36
365	2.91	4.49	5.76	3.71	
365	2.91	4.49	3.84	2.77	
365	2.91	4.49	1.92	1.60	
411	3.03	5.99	0	0.360	
411	3.03	5.99	10.0	4.566	
411	3.03	5.99	8.0	3.77	
411	3.03	5.99	6.0	3.04	4.17
411	3.03	5.99	4.0	2.24	
411	3.03	5.99	2.0	1.324	
411	3.03	5.99	0	0.465	
455	3.24	5.44	0	0.341	
455	3.24	5.44	9.62	3.83	
455	3.24	5.44	7.70	3.09	
455	3.24	5.44	5.77	2.52	3.59
455	3.24	5.44	3.85	1.89	
455	3.24	5.44	1.92	1.05	
455	3.24	5.44	0	0.394	
500	2.81	4.23	0	0.371	
500	2.81	4.23	9.27	3.26	
500	2.81	4.23	7.42	2.74	
500	2.81	4.23	5.56	2.16	3.16
500	2.81	4.23	3.71	1.48	
500	2.81	4.23	1.85	1.00	
500	2.81	4.23	0	0.350	
540	2.46	3.64	0	0.34	
540	2.46	3.64	9.02	3.08	
540	2.46	3.64	7.22	2.51	
540	2.46	3.64	5.41	1.98	2.98
540	2.46	3.64	3.61	1.51	
540	2.46	3.64	1.80	1.03	
540	2.46	3.64	0	0.353	
591	2.73	4.17	0	0.388	
591	2.73	4.17	9.82	3.50	
591	2.73	4.17	7.86	2.91	
591	2.73	4.17	5.90	2.27	3.17
591	2.73	4.17	3.93	1.70	
591	2.73	4.17	1.96	1.03	
591	2.73	4.17	0	0.427	
673	2.42	4.85	0	0.355	
673	2.42	4.85	8.70	3.65	
673	2.42	4.85	6.96	3.05	
673	2.42	4.85	5.22	2.51	3.85
673	2.42	4.85	3.48	1.74	
673	2.42	4.85	1.74	1.06	
673	2.42	4.85	0	0.346	
773	2.10	3.55	0	0.424	
773	2.10	3.55	7.60	4.34	
773	2.10	3.55	6.06	3.57	
773	2.10	3.55	4.54	2.84	5.16
773	2.10	3.55	3.03	2.14	
773	2.10	3.55	1.51	1.33	
773	2.10	3.55	0	0.412	
837	1.94	3.27	0	0.465	
837	1.94	3.27	9.89	6.45	
837	1.94	3.27	7.91	5.31	
837	1.94	3.27	5.94	4.18	6.07
837	1.94	3.27	3.96	3.01	
837	1.94	3.27	1.98	1.90	
837	1.94	3.27	0	0.385	

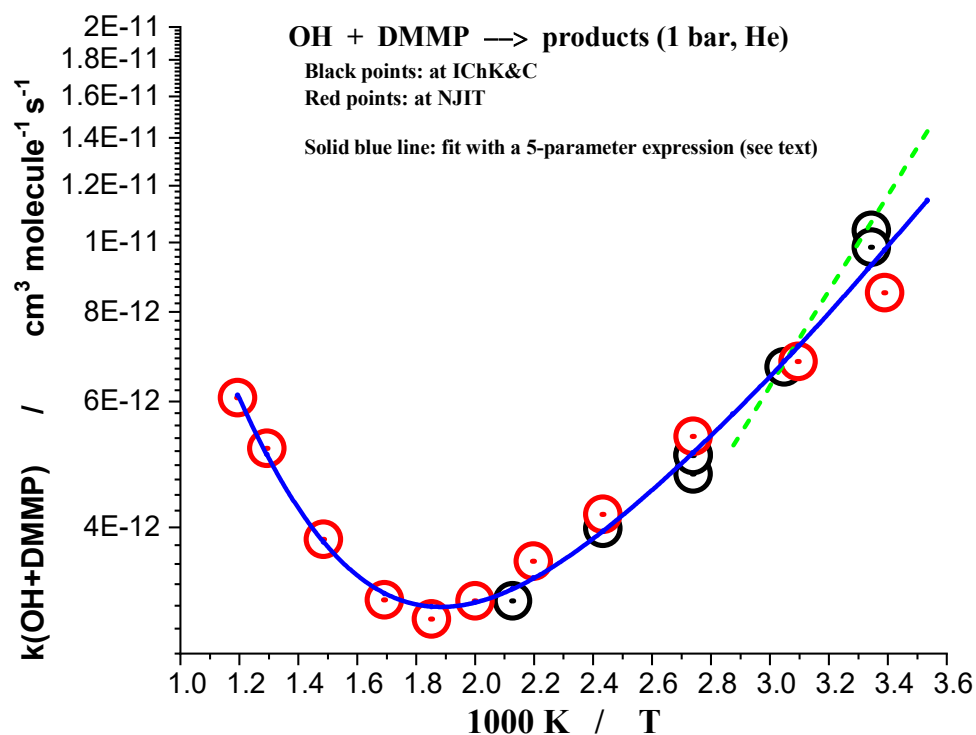


Figure 4. Summary. Rate constant of reaction (1) at 1 bar, over the temperature range 298–837 K. Red points: N₂O/H₂O/He + 193 nm, (at NJIT), black points: O₃/H₂O/He + 266 nm, (at ICKC). Blue line—fit by a 5-parameter expression (see text). Green dotted line: the only previous indirect experimental determination (relative rates method [13]).

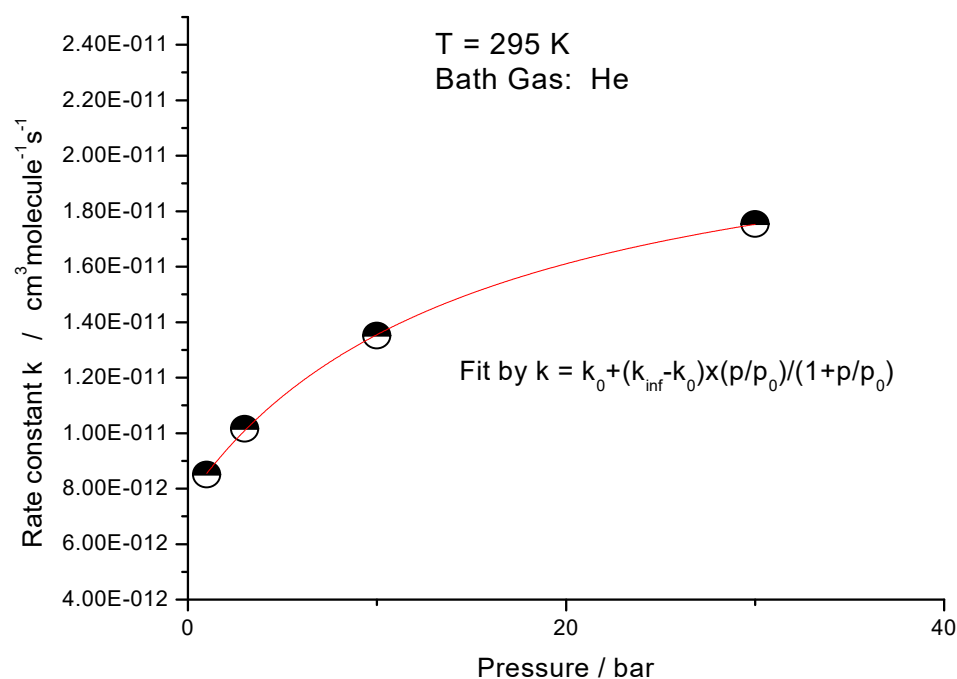
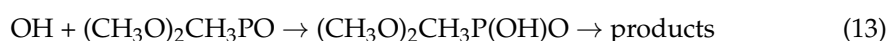
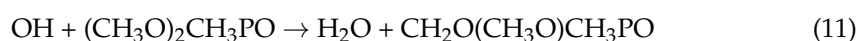


Figure 5. Pressure dependence of the rate constant of reaction (1). Bath gas—He. Temperature 295 K. Smooth curve—fit using a simple model (see text). Fitted parameters: $k_0 = (7.64 \pm 0.12) \times 10^{-12}$ cm³ molecule⁻¹ s⁻¹, $k_{inf} = (2.25 \pm 0.044) \times 10^{-11}$ cm³ molecule⁻¹ s⁻¹, and $p_0 = (15.2 \pm 1.2)$ bar.

4. Discussion

The most prominent feature is the V-shaped temperature dependence of the rate constant—negative at low temperatures, positive at high temperatures, with the turning

point at 530 ± 10 K. There could potentially be two reasons for such peculiar temperature dependence [14]. One possibility is that the ground state of the transition state lies below the ground state of the reactants (“negative barrier”, “submerged barrier” [16,26]. In such a case the modified transition state theory predicts V-shaped temperature dependence, negative at low temperatures, and positive at high temperatures, with possible pressure dependence at high pressures [16,26]. Another possibility is that the reaction has two or more channels, like direct H-atom abstraction from methoxy $\text{CH}_3\text{-O-}$ groups, methyl group $\text{CH}_3\text{-}$ as well as attachment of OH to the double P=O bond in DMMP:



Neither theoretical works on the abstraction channels (11) and (12), nor any theoretical works on the prospective complex forming channel (13) with further transformations within the complex are currently available. Complex forming reactions often have negative temperature dependence; typical H-atom abstraction reactions usually have small positive barriers [27]. Theoretical calculations for the reaction of OH with trimethyl phosphate resulted in the “negative barriers” for several conformers of the transition state of the channel of H-atom abstractions from methoxy groups [28]. The analysis of the reaction products in the study in solutions by pulsed radiolysis [17] led to the conclusion that both the H-atom abstraction from the methyl group, channel (12), and attachment to the double bond, channel (13), are not important, thus that the only important channel is abstraction of H-atom from methoxy groups. This channel energetically should be similar to that in the reaction of OH with trimethyl phosphate, and is expected to have a submerged barrier. The experimental observations of this work (V-shaped temperature dependence and pressure dependence) support such an assumption.

5. Conclusions

The kinetics of the reaction of hydroxyl radical with dimethyl methylphosphonate, DMMP, (reaction (1)) was studied using direct techniques by two groups using two different methods of generation of hydroxyl radicals over an extended temperature range of 273–837 K.

The room temperature rate constant is in reasonable agreement with the only previous indirect determination [17].

A V-shaped temperature dependence, negative at low temperatures, and positive at higher temperatures, with a turning point at 530 ± 10 K, was unambiguously established.

Significant dependence of the rate constant on the bath gas pressure (He) was observed. The observations are consistent with the assumption that the major channel of this reaction is abstraction of H-atom from methoxy groups, in which the reaction barrier lies below the ground state of the reactants.

This study is the first direct study of the title reaction. Wide temperature range allowed revealing the peculiar V-shaped temperature dependence. This is the second reaction of hydroxyl radicals with an organophosphorus compound that exhibits such behavior.

It is apparent that extended experimental (including bath gas pressure dependence over extended pressure and temperature ranges) as well as theoretical studies of this and other elementary reactions of this class, are required for better understanding of the mechanism of these reactions.

Author Contributions: Investigation—X.Z., D.A.B., P.V.K., I.E.G., E.N.C., L.N.K.; writing—review and editing—X.Z., P.V.K., E.N.C., L.N.K.; supervision—E.N.C., L.N.K.; writing—original draft—L.N.K. All authors have read and agreed to the published version of the manuscript.

Funding: This research was funded by a grant from the Russian Science Foundation (grant No. 19-73-20060).

Institutional Review Board Statement: Not applicable.

Informed Consent Statement: Not applicable.

Acknowledgments: The study performed at ICKC (Novosibirsk) was supported by a grant from the Russian Science Foundation (grant No. 19-73-20060).

Conflicts of Interest: The authors declare no conflict of interest.

References

1. Baranov, A.N. *Combustion-Fire-Explosion-Safety*; Ministry of Russian Federation for Civil Defence, Emergencies and Elimination of Consequences of Natural Disasters (FGU VNIPO EMERCOM of Russia): Moscow, Russia, 2004; p. 364.
2. Hastie, J.W.; Bonnell, D.W. *Molecular Chemistry of Inhibited Combustion Systems*; National Bureau of Standards: Gaithersburg, MD, USA. [[CrossRef](#)]
3. Tapscott, R.E.; Sheinson, R.S.; Babushok, V.; Nyden, M.R.; Gann, R.G. Alternative Fire Suppressant Chemicals: A Research Review with Recommendations. *NIST Tech. Note.* **2001**, *1443*, 13.
4. Korobeinichev, O.P.; Shvartsberg, V.M.; Chernov, A.A. The Destruction Chemistry of Organophosphorus Compounds in Flames—II: Structure of a Hydrogen–Oxygen Flame Doped with Trimethylphosphate. *Combust. Flame* **1999**, *118*, 727–732. [[CrossRef](#)]
5. Glaude, P.A.; Melius, C.; Pitz, W.J.; Westbrook, C.K. Detailed Chemical Kinetic Reaction Mechanisms for Incineration of Organophosphorus and Fluoro-Organophosphorus Compounds. *Proc. Combust. Inst.* **2002**, *29*, 2469–2476. [[CrossRef](#)]
6. Jayaweera, T.M.; Melius, C.F.; Pitz, W.J.; Westbrook, C.K.; Korobeinichev, O.P.; Shvartsberg, V.M.; Shmakov, A.G.; Rybitskaya, I.V.; Curran, H.J. Flame Inhibition by Phosphorus-Containing Compounds over a Range of Equivalence Ratios. *Combust. Flame* **2005**, *140*, 103–115. [[CrossRef](#)]
7. Korobeinichev, O.P.; Shvartsberg, V.M.; Chernov, A.A.; Mokrushin, V.V. Hydrogen-Oxygen Flame Doped with Trimethyl Phosphate, its Structure and Trimethyl Phosphate Destruction Chemistry. *Symp. Combust.* **1996**, *26*, 1035–1042. [[CrossRef](#)]
8. Twarowski, A.J. The Influence of Phosphorus Oxides and Acids on Rate of H+OH Recombination. *Combust. Flame* **1993**, *94*, 91–107. [[CrossRef](#)]
9. Korobeinichev, O.P.; Bolshova, T.A.; Shvartsberg, V.M.; Chernov, A.A. Inhibition and Promotion of Combustion by Organophosphorus Compounds Added to Flames of CH₄ or H₂ in O₂ and Ar. *Combust. Flame* **2001**, *125*, 744–751. [[CrossRef](#)]
10. Glaude, P.A.; Curran, H.J.; Pitz, W.J.; Westbrook, C.K. Kinetic Study of the Combustion of Organophosphorus Compounds. *Proc. Combust. Inst.* **2000**, *28*, 1749–1756. [[CrossRef](#)]
11. Azam, H.M.; Alam, T.; Hasan, M.; Yameogo, D.D.S.; Kannan, A.D.; Rahman, A.; Kwon, M.J. Phosphorous in the environment: Characteristics with distribution and effects, removal mechanisms, treatment technologies, and factors affecting recovery as minerals in natural and engineered systems. *Environ. Sci. Pollut. Res. Int.* **2019**, *26*, 20183–20207. [[CrossRef](#)]
12. Tuazon, E.C.; Atkinson, R.; Aschumann, S.M.; Arey, J.; Winer, A.M.; Pitts, J.N., Jr. Atmospheric Loss Processes of 1,2-Dibromo-3-Chloropropane and Trimethyl Phosphate". *Environ. Sci. Technol.* **1986**, *20*, 1043–1046. [[CrossRef](#)]
13. Aschmann, S.M.; Long, W.D.; Atkinson, R. Rate Constants for the gas-phase reactions of OH radicals with dimethyl phosphonate over the temperature range of 278–351 K and for a series of other organophosphorus compounds at similar to 280 K. *J. Phys. Chem. A* **2008**, *112*, 4793–4799. [[CrossRef](#)] [[PubMed](#)]
14. Koshlyakov, P.V.; Barkova, D.A.; Gerasimov, I.E.; Chesnokov, E.N.; Zhang, X.; Krasnoperov, L.N. Kinetics of the gas-phase reaction of hydroxyl radicals with trimethyl phosphate over the 273–837 K temperature range. *RSC Adv.* **2021**, *11*, 14121–14131. [[CrossRef](#)]
15. Krasnoperov, L.N.; Peng, J.; Marshall, P. Modified Transition State Theory and Negative Apparent Activation Energies of Simple Metathesis Reactions. In Proceedings of the 16th International Symposium on Gas Kinetics, Cambridge, UK, 23–27 July 2000; p. PA9.
16. Krasnoperov, L.N.; Peng, J.; Marshall, P. Modified Transition State Theory and Negative Apparent Activation Energies of Simple Metathesis Reactions: Application to the Reaction CH₃ + HBr → CH₄ + Br. *J. Phys. Chem. A* **2005**, *110*, 3110–3120. [[CrossRef](#)] [[PubMed](#)]
17. Aguila, A.; O’Shea, K.E.; Tobien, T.; Asmus, K.-D. Reactions of Hydroxyl Radical with Dimethyl Methylphosphonate and Diethyl Methylphosphonate. A Fundamental Mechanistic Study. *J. Phys. Chem. A* **2001**, *105*, 7834–7839. [[CrossRef](#)]
18. Dunlea, E.J.; Ravishankara, A.R. Kinetic Studies of the Reactions of O(¹D) with Several Atmospheric Molecules. *Phys. Chem. Chem. Phys.* **2004**, *6*, 2152–2161. [[CrossRef](#)]
19. Dunlea, E.J.; Ravishankara, A.R. Measurement of the Rate Coefficient for the Reaction of O(1D) with H₂O and Re-Evaluation of the Atmospheric OH Production Rate. *Phys. Chem. Chem. Phys.* **2004**, *6*, 3333–3340. [[CrossRef](#)]
20. Zhang, X.; Sangwan, M.; Yan, C.; Koshlyakov, P.V.; Chesnokov, E.N.; Bedjanian, Y.; Krasnoperov, L.N. Disproportionation Channel of the Self-reaction of Hydroxyl Radical, OH + OH → H₂O + O, Revisited. *J. Phys. Chem. A* **2020**, *124*, 3993–4005. [[CrossRef](#)]
21. Sangwan, M.; Chesnokov, E.N.; Krasnoperov, L.N. Reaction OH + OH Studied over the 298–834 K Temperature and 1–100 bar Pressure Ranges. *J. Phys. Chem. A* **2012**, *116*, 6282–6294. [[CrossRef](#)]
22. Sangwan, M.; Krasnoperov, L.N. Disproportionation Channel of Self-Reaction of Hydroxyl Radical, OH + OH → H₂O + O, Studied by Time-Resolved Oxygen Atom Trapping. *J. Phys. Chem. A* **2012**, *116*, 11817–11822. [[CrossRef](#)]

23. Yan, C.; Kocevskaja, S.; Krasnoperov, L.N. Kinetics of the Reaction of CH₃O₂ Radicals with OH Studied over the 292–526 K Temperature Range. *J. Phys. Chem. A* **2016**, *120*, 6111–6121. [[CrossRef](#)]
24. Sangwan, M.; Krasnoperov, L.N. Kinetics of the Gas Phase Reaction CH₃ + HO₂. *J. Phys. Chem. A* **2013**, *117*, 2916–2923. [[CrossRef](#)] [[PubMed](#)]
25. Sangwan, M.; Yan, C.; Chesnokov, E.N.; Krasnoperov, L.N. Reaction CH₃ + CH₃ → C₂H₆ Studied over the 292–714 K and 1–100 bar Pressure Ranges. *J. Phys. Chem. A* **2015**, *119*, 7847–7857. [[CrossRef](#)] [[PubMed](#)]
26. Gao, Y.; Alecu, I.M.; Hsieh, P.-C.; Morgan, B.P.; Marshall, P.; Krasnoperov, L.N. Thermochemistry Is Not a Lower Bound to the Activation Energy of Endothermic Reactions: A Kinetic Study of the Gas-Phase Reaction of Atomic Chlorine with Ammonia. *J. Phys. Chem. A* **2006**, *110*, 6844–6850. [[CrossRef](#)] [[PubMed](#)]
27. Manion, J.A.; Huie, R.E.; Levin, R.D., Jr.; Burgess, D.R.; Orkin, V.L.; Tsang, W.; McGivern, W.S.; Hudgens, J.W.; Knyazev, V.D.; Atkinson, D.B.; et al. *NIST Chemical Kinetics Database, NIST Standard Reference Database 17, Version 7.0 (Web Version)*, Release 1.4.3, Data version 2008.12; National Institute of Standards and Technology: Gaithersburg, MD, USA, 2008; pp. 20899–28320.
28. Burns, D.S.; Cory, M.G.; Taylor, D.E.; Bunte, S.W.; Runge, K.; Vasey, J.L. A Comparison of Primary and Secondary Hydrogen Abstraction from Organophosphates by Hydroxyl Radical. *Int. J. Chem. Kinet.* **2013**, *45*, 187–201. [[CrossRef](#)]